Hydrolysis of ionic clusters to induce interconnective sieving pores in ion-conductive membranes for vanadium flow batteries

Bo Pang[1], Zihao Fan[1], Wanting Chen[1], Xiaoming Yan[1], Ruohan Du[1], Xiaozhou Wang[1], Xuemei Wu[1], Fujun Cui[2], Minggang Guo[2], Gaohong He[1,2]**

1 State Key Laboratory of Fine Chemicals, Research and Development Center of Membrane Science and Technology, School of Chemical Engineering, Dalian University of Technology, Dalian, 116024, China.

2 Panjin Institute of Industrial Technology, Liaoning Key Laboratory of Chemical Additive Synthesis and Separation, Dalian University of Technology, Panjin 124221, Liaoning, China

*Xuemei Wu: xuemeiw@dlut.edu.cn, hgaohong@dlut.edu.cn

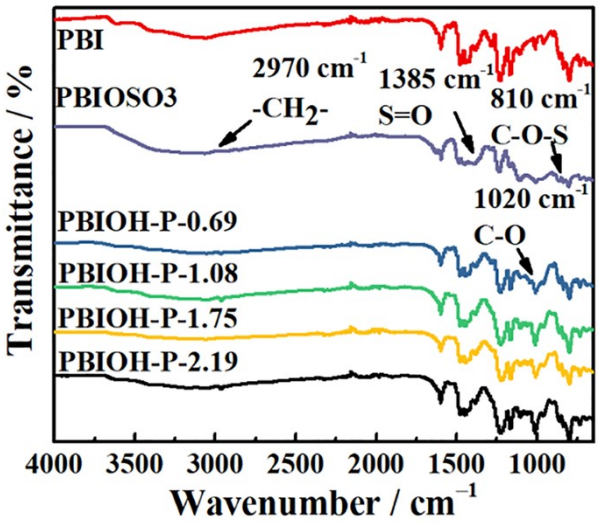

Fig. S1. The FTIR patterns of PBI, PBIOSO3 and PBIOH-P membranes.

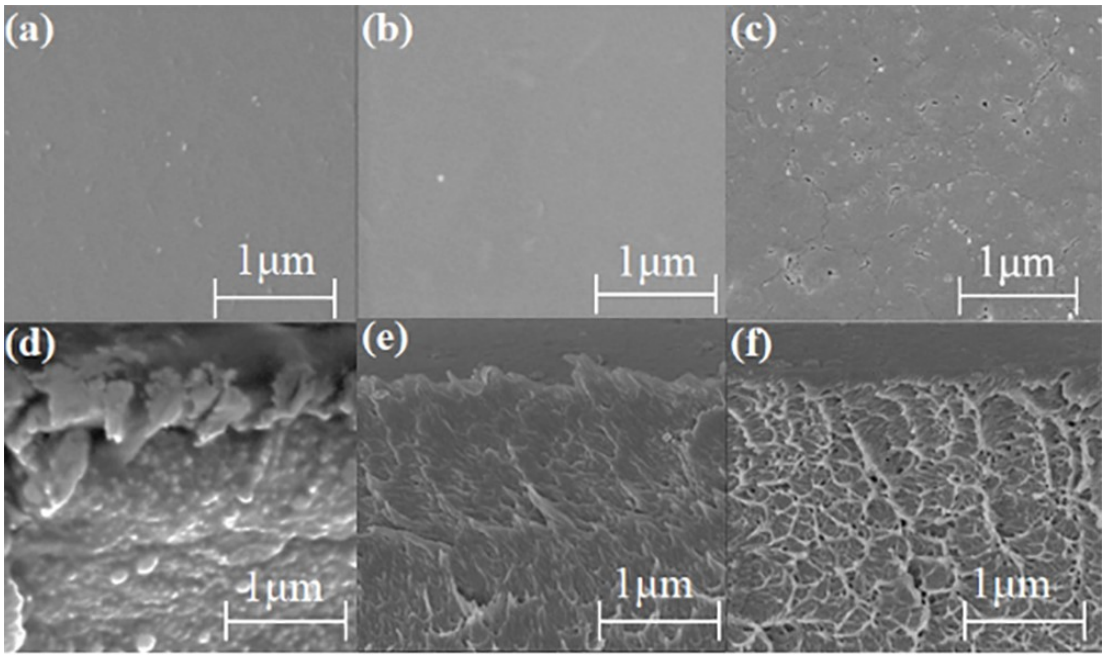

Fig. S2. The SEM surface images of (a) PBI, (b) PBIOSO3 and (c) PBIOH-P-1.75 membranes; cross-section images of (d) PBI, (e) PBIOSO3 and (f) PBIOH-P-1.75 membranes.

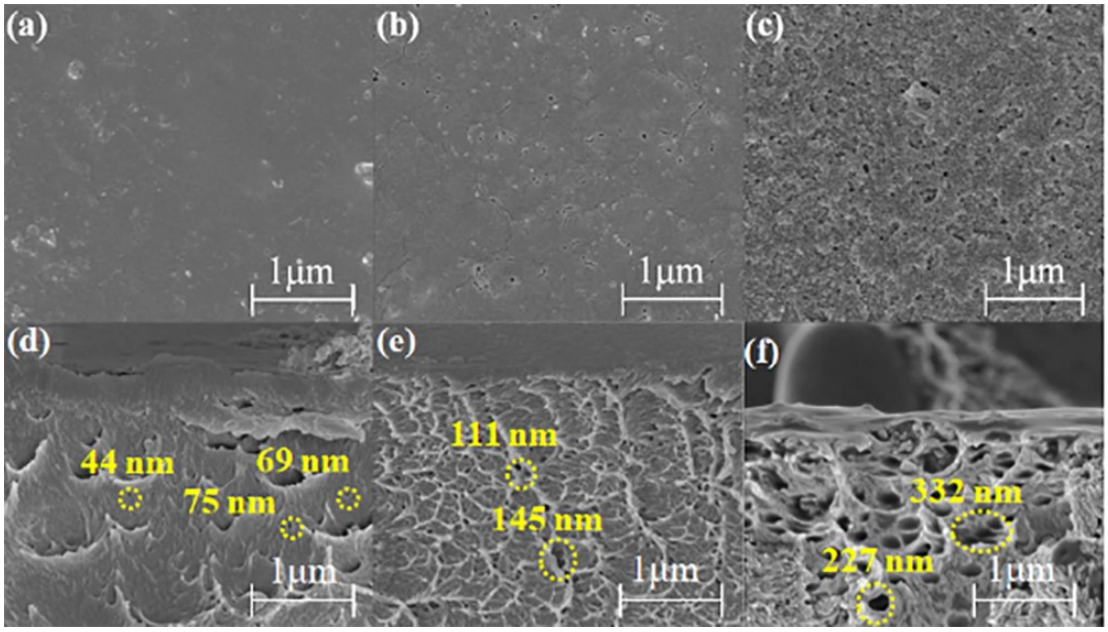

Fig. S3. The SEM surface images of (a) PBIOH-P-0.69, (b) PBIOH-P-1.75 and (c) PBIOH-P-2.19 membranes; cross-section images of (d) PBIOH-P-0.69, (e) PBIOH-P-1.75 and (f) PBIOH-P-2.19 membranes

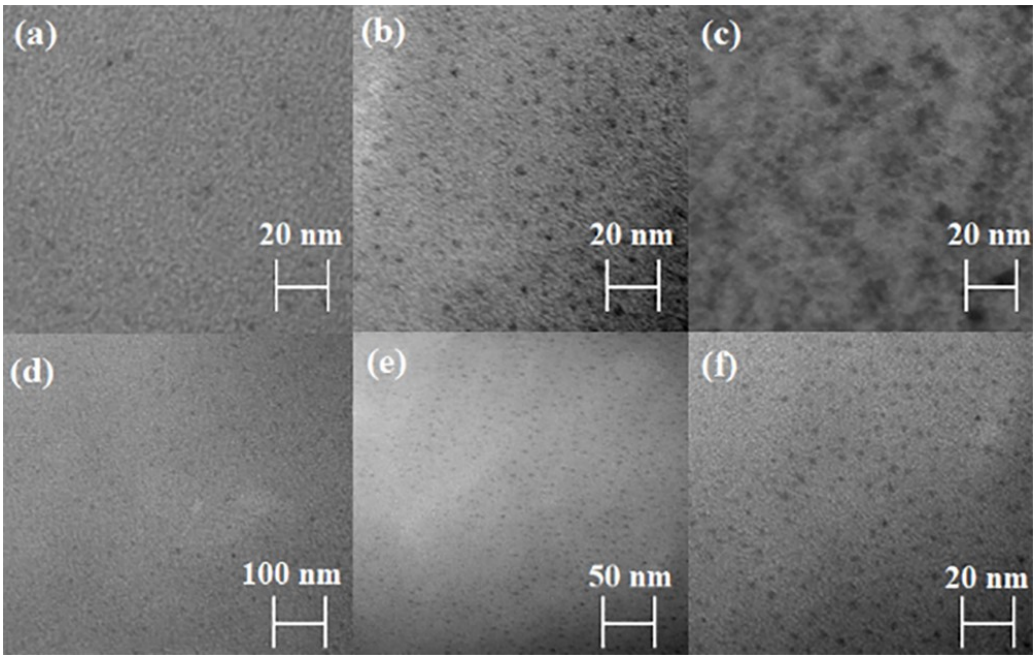

Fig. S4. The TEM ions clusters images of (a) OPBIOSO3-0.69, (b) OPBIOSO3-1.75 and (c) OPBIOSO3-2.19 membranes; TEM ions clusters images of OPBIOSO3-1.75 membrane with 100 nm, 50 nm and 20 nm.

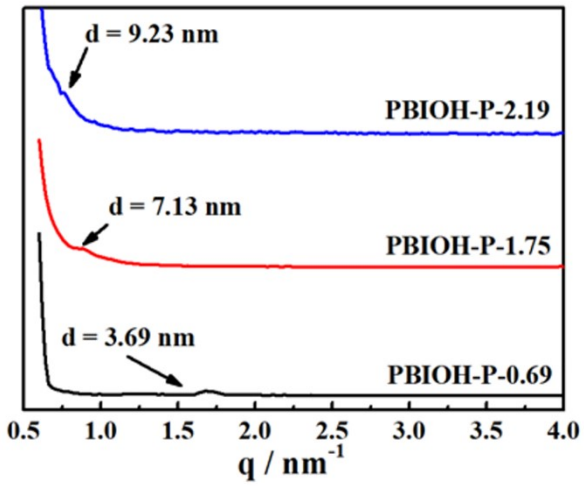

Fig. S5. SAXS curves of the PBIOH-P membranes.

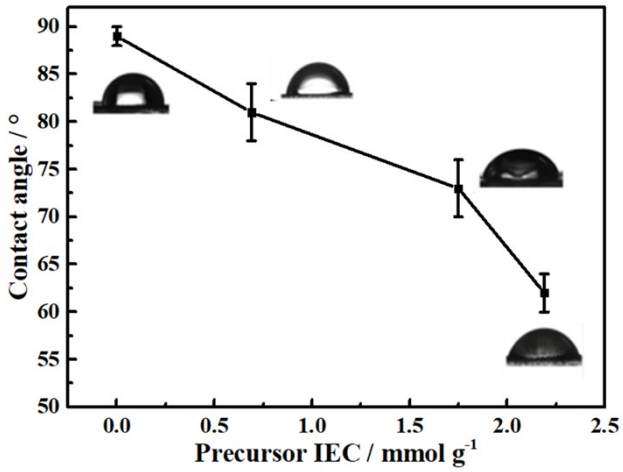

Fig. S6. The contact angle of the PBI and PBIOH-P membranes.

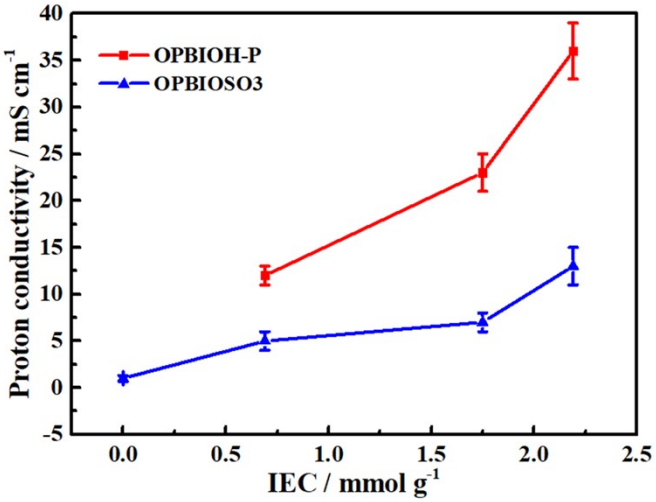

Fig. S7. The proton conductivity of the PBIOH-P and PBIOSO3 membranes.

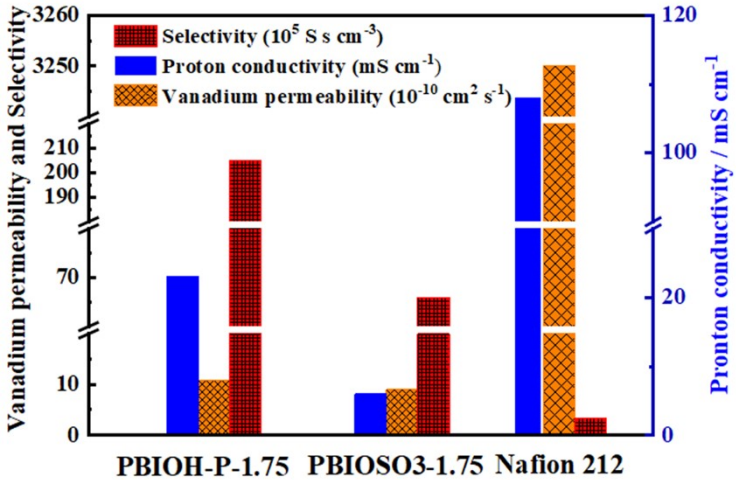

Fig. S8. The Selectivity, proton conductivity and vanadium permeability of the PBIOH-P, PBIOSO3-1.75 and Nafion 212 membranes. (Selectivity is denoted as proton conductivity divided by vanadium permeability)

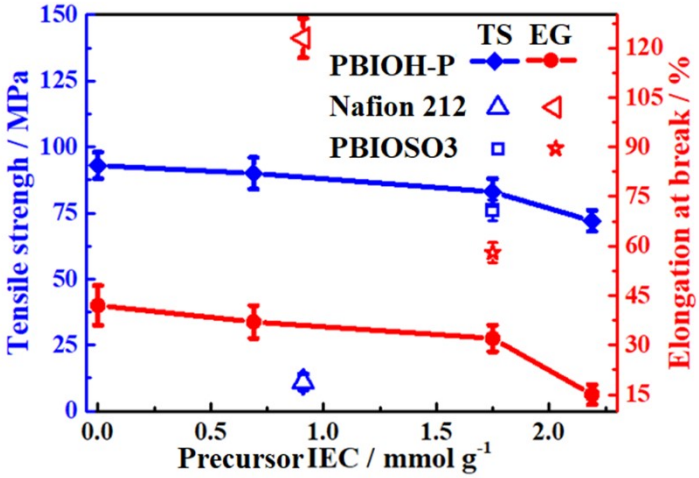

Fig. S9. Tensile strength and elongation at break of the PBIOH-P and PBIOSO3 membranes with precursor IEC of 1.75, and Nafion 212 membrane.

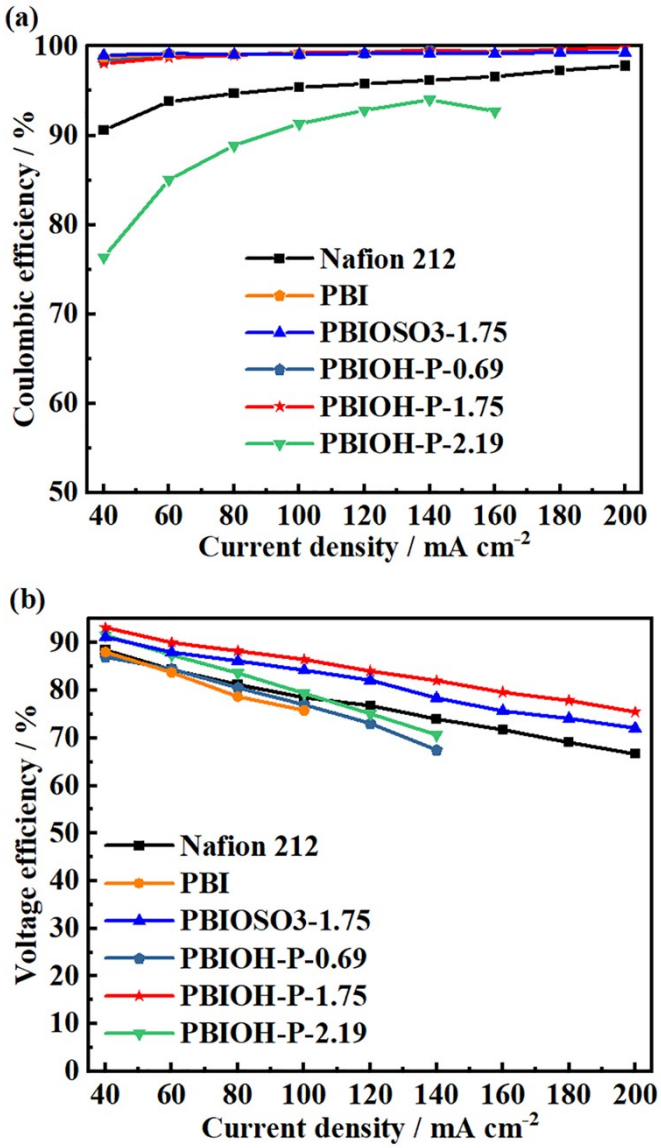

Fig. S10. Columbic efficiency and voltage efficiency of the PBIOH-P, Nafion 212, PBI and PBIOSO3-1.75 based cells.

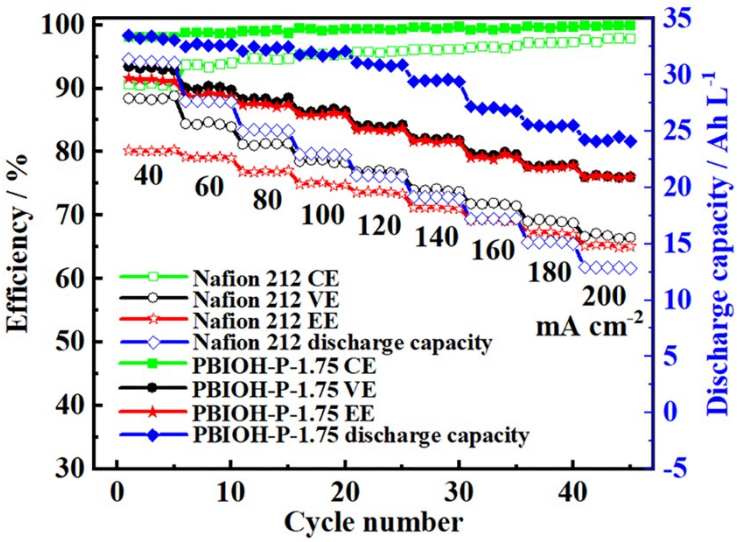

Fig. S11. The rate performance of the PBIOH-P-1.75 and Nafion 212 based VFBs.

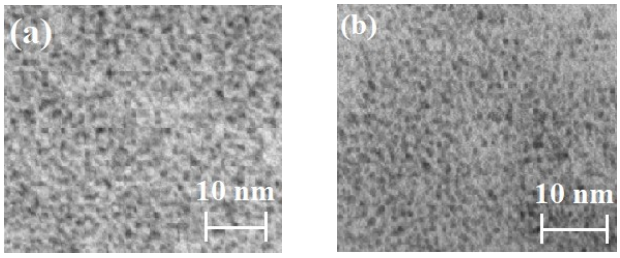

Fig. S12. *The TEM images of pore morphology (a) before and (b) after VFB cycling test*

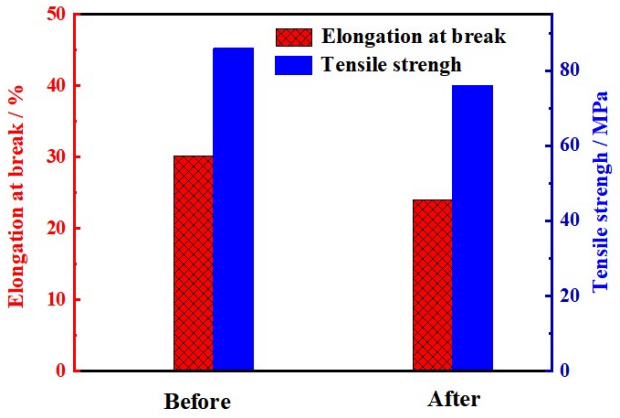

Fig. S13. *The mechanical properties before and after VFB cycling test*

Table S1 The comparison of H^+/V^{n+} ion selectivity with recently reported porous membranes, composite membranes, and anion exchange membranes

Membranes	*Category*	*H^+/V^{n+} Selectivity*	*Conductivity*	*Reference*

		$\times 10^5$ S min cm^{-3}	mS cm^{-1}	
This work	Porous membranes	3.42	70	
SPEEK/ SPAES-15	Composite membrane	0.29	29.3	1
SPI/2% PMPP	Composite membrane	1.42	116	2
SPEEK/Him-pS-3	Composite membrane	0.40	31.54	3
S/801&808-4	Composite membrane	2.2	78	4
SPEEK/SPPTA-25	Composite membrane	0.23	29.08	5
QCPPAE	Anion exchange membrane	0.96	21	6
CAPSU	Anion exchange membrane	2.08	15	7
PyPPSU	Anion exchange membrane	2.44	8.8	8
PVDF/SiO_2-SO_3H-42	Porous membranes	1.25	14	9
2# ABPBI	Porous	0.79	30	10

Reference:

1. P. Qian, H. Wang , L. Zhang, Y. Zhou, H. Shi, An enhanced stability and efficiency of SPEEK-based composite membrane influenced by amphoteric side-chain polymer for vanadium redox flow battery, J. Membr. Sci. 2022, **643**, 120011.

2. M. Zhang, G. Wang, A. Li, X. Wei, F. Li, J. Zhang, J. Chen, R. Wang, Novel sulfonated polyimide membrane blended with flexible poly[bis (4-methylphenoxy) phosphazene] chains for all vanadium redox flow battery, J. Membr. Sci. 2021, **619**, 118800.

*3. D. Zhang, Z. Xu, X. Zhang, L. Zhao, Y. Zhao, S. Wang, W. Liu, X. Che, J. Yang, J. Liu, C. Yan, Oriented Proton-Conductive Nanochannels Boosting a Highly Conductive Proton-Exchange Membrane for a Vanadium Redox Flow Battery, ACS Appl. Mater. Interfaces. 2021, **13**, 4051-4061.*

*4. L. Xin, D. Zhang, K. Qu, Y. Lu, Y. Wang, K. Huang, Z. Wang, W. Jin, Z. Xu, Zr-MOF-Enabled Controllable Ion Sieving and Proton Conductivity in Flow Battery Membrane, Adv. Funct. Mater. 2021, **31**, 2104629.*

5. P. Qian, H. Wang, Y. Jiang, Y. Zhou, H. Shi, High-performance composite membrane based on synergistic main-chain/side-chain proton conduction channels for the vanadium redox flow battery, J. Mater. Chem. A,2021, 9,4240-4252.

*6. M. Cha, J. Lee, T. Kim, H. Jeong, H. Shin, S. Oh, Y. Hong, Preparation and characterization of crosslinked anion exchange membrane (AEM) materials with poly(phenylene ether)-based short hydrophilic block for use in electrochemical applications, J Membr Sci. 2017, **530**,73–83.*

*7. M. Cha, H. Jeong, H. Shin, S. Hong, T. Kim, S. Oh, J. Lee, Y Hong, Crosslinked anion exchange membranes with primary diamine-based crosslinkers for vanadium redox flow battery application, J Power Sources 2017, **363**, 78–86.*

*8. B. Zhang, E. Zhang, G. Wang, P. Yu, Q. Zhao, F. Yao, Poly(phenyl sulfone) anion exchange membranes with pyridinium groups for vanadium redox flow battery applications, J Power Sources, 2015, **282**,328–334.*

9. L. Ling, M. Xiao, D. Han, S. Ren, S. Wang, Y. Meng, Porous composite membrane of PVDF/Sulfonic silica with high ion selectivity for vanadium redox flow battery, J. Membr. Sci. 2019, **585**, 230-237.

10. T. Luo, B. Dreusicke, M. Wessling, Tuning the ion selectivity of porous poly(2,5-benzimidazole) membranes by phase separation for all vanadium redox flow batteries, J. Membr. Sci. 2018, **556**, 164-177.